Gravitational Waves and Primordial Black Hole Productions from Gluodynamics

Song He[1,2],* Li Li[3,4,5],† Zhibin Li[6],‡ and Shao-Jiang Wang[3]§

[1] *Center for Theoretical Physics and College of Physics, Jilin University, Changchun 130012, China*
[2] *Max Planck Institute for Gravitational Physics (Albert Einstein Institute), Am Muhlenberg 1, 14476 Golm, Germany*
[3] *CAS Key Laboratory of Theoretical Physics, Institute of Theoretical Physics, Chinese Academy of Sciences, Beijing 100190, China*
[4] *School of Fundamental Physics and Mathematical Sciences, Hangzhou Institute for Advanced Study, University of Chinese Academy of Sciences, Hangzhou 310024, China*
[5] *Peng Huanwu Collaborative Center for Research and Education, Beihang University, Beijing 100191, China. and*
[6] *School of Physics and Microelectronics, Zhengzhou University, Zhengzhou 450001, China*

We construct a holographic model describing the gluon sector of Yang-Mills theories at finite temperature in the non-perturbative regime. The equation of state as a function of temperature is in good accordance with the lattice quantum chromodynamics (QCD) data. Moreover, the Polyakov loop and the gluon condensation, which are proper order parameters to capture the deconfinement phase transition, also agree quantitatively well with the lattice QCD data. We obtain a strong first-order confinement/deconfinement phase transition at $T_c = 276.5\,\mathrm{MeV}$ that is consistent with the lattice QCD prediction. The resulting stochastic gravitational-wave backgrounds from this confinement/deconfinement phase transition are obtained with potential detectability in the International Pulsar Timing Array and Square Kilometre Array in the near future when the associated productions of primordial black holes (PBHs) saturate the current observational bounds on the PBH abundances from the LIGO-Virgo-Collaboration O3 data.

Introduction— The early Universe before the big bang nucleosynthesis is opaque to electromagnetic waves. Thanks to the recent gravitational-wave (GW) detections, future observations of stochastic GW backgrounds (SGWBs) would reveal the new physics [1–4] from the early Universe, including various first-order phase transitions (FOPTs) beyond the standard model (SM) of particle physics (see [5] and references therein for a model summary). It was recently found that the FOPT not only associates with SGWBs, but also produces primordial black holes (PBHs) in general [6, 7] (see also [8] for an explicit example from the electroweak PT), regardless of the specific particle physics model for realizing the FOPTs (see also [9–13] for other specific mechanisms of PBH productions during some particular kinds of FOPTs). In particular, for the FOPT around the quantum chromodynamics (QCD) scale, the associated SGWBs can be probed by the Pulsar Timing Array (PTA) and Square Kilometre Array (SKA) observations, and the associated PBH abundance could be constrained by the LIGO-Virgo-Collaboration (LVC) network. Since the QCD PT in SM is cross-over, we study pure gluons in this Letter for a realization of the FOPT around the QCD scale with associated productions of SGWBs and PBHs.

On the other hand, investigating the pure gluon system is important to understand the nature of hot and dense QCD matter formed in the early universe and the laboratory. In particular, the gluon dynamics is dominant during 10^{-5} seconds into the expansion of the early Universe [14–17] and an extremely rapid thermalization [18–20] in nucleus-nucleus collisions. On theoretical side, the thermodynamics of the pure-gauge sector can be relevant to capture the essential qualitative features of the deconfinement, which is characterized by center symmetry and shows all the infrared difficulties of QCD. Due to the famous asymptotic freedom, non-perturbative approaches are necessary for quantitative studies of its dynamics. In addition to the lattice QCD that relies on massive computing power, an alternative non-perturbative approach is to employ the gauge/gravity correspondence [21–23] that provides a powerful way to study strongly coupled non-Abelian gauge theories (earlier studies on the pure gluon system from holography can be found, for example, in Refs. [24–27]).

In this Letter, we provide a bottom-up holographic QCD model for the pure gluon QCD system in Einstein-Dilaton theory. The equation of state (EoS) quantitatively match the pure gluon system in lattice QCD [28, 29]. The confinement PT in gauge theory is characterized by the Polyakov loop operator $\langle \mathcal{P} \rangle$ which is finite in the deconfined phase and becomes vanishing in the confined phase for pure gluon [30, 31]. The temperature dependence of $\langle \mathcal{P} \rangle$ from our model matches the lattice simulation [32] perfectly, and the predicted critical temperature $T_c = 276.5\,\mathrm{MeV}$ agrees with the expectation in the literature [28, 33]. Moreover, another important quantity characterizing the deconfinement PT in pure gluon system is the gluon condensation, which can be computed to be quantitatively consistent with the trace anomaly [28]. The strong FOPT in the early universe is also a potentially important source for the productions of SGWBs and PBHs. Our present model provides a scenario for generating GWs from a FOPT within the SM of particle physics. We find that the resulting GW signals could be detected in the upcoming International PTA (IPTA) and SKA observations for the associated PBH abundance saturating the current observational bounds from the LVC constraints.

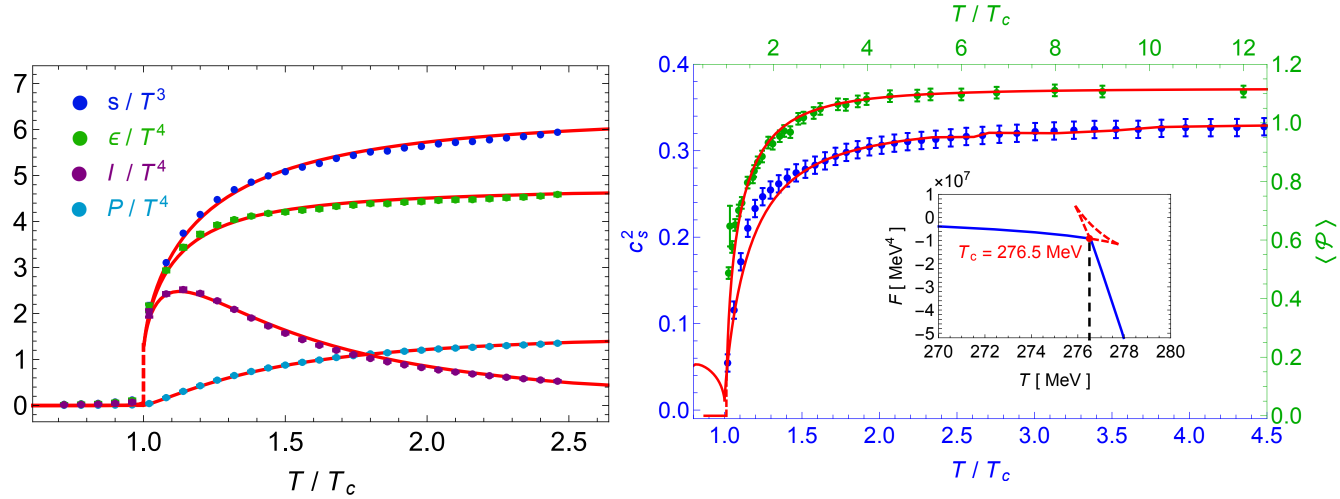

FIG. 1. The comparison between the lattice data (with error bar) of the pure gluon thermodynamics and our holographic calculations (solid curves) on various thermodynamic quantities. **Left panel:** The temperature dependence of the energy density ϵ, the entropy density s, the pressure P, and the trace anomaly $I = (\epsilon - 3P)$ [29]. **Right panel:** The squared speed of sound $c_s^2 \equiv dP/d\epsilon$ [28] and the Polyakov loop $\langle \mathcal{P} \rangle$ [32] in function of temperature. **Insert:** The free energy density F with respect to the temperature from our model. There is a first-order confinement/deconfinement PT at $T_c = 276.5\,\mathrm{MeV}$.

Model— We now build up a holographic model for the pure gluon system with the action of the following form.

$$S = \frac{1}{2\kappa_N^2} \int \mathrm{d}^5 x \sqrt{-g} \left[\mathcal{R} - \frac{1}{2} \nabla_\mu \phi \nabla^\mu \phi - V(\phi) \right] \tag{1}$$

with the minimal cost of degrees of freedom to capture the essential dynamics. The gravitational theory includes only two fields: the spacetime metric $g_{\mu\nu}$, and a real scalar ϕ with its profile breaking conformal invariance that can be understood roughly as the running coupling of QCD. In addition to κ_N^2 that is the effective Newton constant, the potential $V(\phi)$ will be fixed by matching to the lattice QCD data.

The black hole with non-trivial scalar hair reads

$$\mathrm{d}s^2 = -f(r) e^{-\eta(r)} \mathrm{d}t^2 + \frac{\mathrm{d}r^2}{f(r)} + r^2 \mathrm{d}\mathbf{x}_3^2, \quad \phi = \phi(r)\,, \tag{2}$$

with $\mathrm{d}\mathbf{x}_3^2 = \mathrm{d}x^2 + \mathrm{d}y^2 + \mathrm{d}z^2$ and r the holographic radial coordinate. The next goal is to find a potential V that can reproduce the EoS of $N_c = 3$ pure gluon QCD. Thermodynamic quantities can be obtained straightforwardly using the standard holographic dictionary, see appendix for more details. It comes as a nice surprise that the simple potential

$$V(\phi) = \left(6\gamma^2 - \frac{3}{2} \right) \phi^2 - 12 \cosh(\gamma\phi) \tag{3}$$

with $\gamma = 0.735$ can reproduce the thermodynamics of lattice data for the pure gluon QCD [28, 29, 32] as shown in Fig. 1 [34]. Remarkably, although the error bars of the up-to-date lattice simulation [29] are tiny, our theoretical results for EoS in the left panel are almost within these error bars. It is obvious from the free energy density F that a strong FOPT takes place at the temperature $T_c = 276.5$ MeV. We also compare the speed of sound c_s in the right panel of Fig. 1. Since c_s is not provided in [29], we use the early data from lattice QCD [28] and find good agreement.

To understand the nature of the FOPT, we compute the expectation value of the Polyakov loop operator $\langle \mathcal{P} \rangle$, which is a good order parameter to the de-confinement PT for pure gluon system [35]. Surprisingly, $\langle \mathcal{P} \rangle$ by our holographic model quantitatively agrees with the lattice data [32] above T_c and it quickly drops to zero below T_c, see the right panel of Fig. 1. It suggests that the FOPT from our model is a confinement/deconfinement PT. Remarkably, the temperature dependence of the gluon condensation $\delta \left\langle \frac{\beta(g)}{2g} G^2 \right\rangle_T$ capturing the deconfinement PT is computed in our holographic model and is found to be coincides with the trace anomaly $\epsilon - 3p$ from EoS, see Fig. 2. Therefore, at T_c, we can then read off some essential quantities that are important to compute the SGWB and PBH productions associated with our FOPT.

Independent of details of any specific particle physics model, the PBH production is a universal consequence of the FOPT [6]. Due to the stochastic nature of bubble nucleations during FOPTs, the progress of populating true-vacuum bubbles in the false-vacuum background is a asynochronized process. There is always a non-vanishing probability to find some Hubble-sized regions to stay in the false vacuum for slightly longer period of time than average. Since the radiation energy density should be

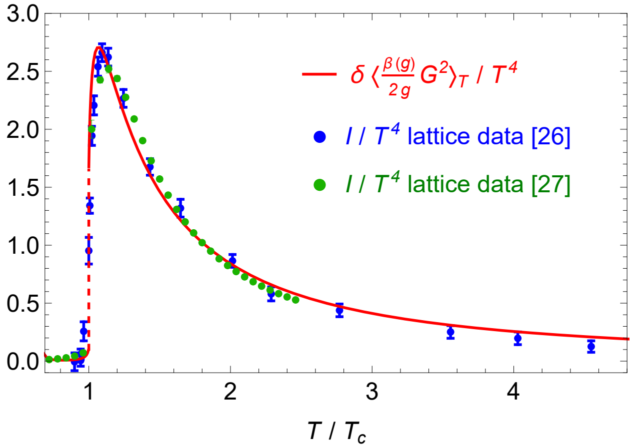

FIG. 2. The temperature dependence of the gluon condensation $\delta\left\langle\frac{\beta(g)}{2g}G^2\right\rangle_T$ of our pure gluon model, where $\beta(g)$ is the β-function with β the QCD gauge coupling. The data with error bar denotes the trace anomaly $I=(\epsilon-3P)$ from lattice QCD [28, 29].

rapidly diluted relative to the vacuum energy density in an expanding Universe, these Hubble-size regions would eventually accumulate enough overdensities in total energy density to finally reach the threshold of PBH productions. What is remarkably for this general mechanism of PBH productions during FOPTs is that the probability to find such Hubble-sized regions with postponed vacuum-decay progress can be made of particular observational interest for both detections from GWs and PBHs, which will be briefly described shortly below and detailed in the supplemental appendix.

GW productions— From the behavior of the free energy density in the insert of the right panel of Fig. 1, it clearly indicates the occurrence of a first-order confinement/deconfinement PT around the critical temperature $T_c=276.5\,\mathrm{MeV}$, which could be a potentially important source for GWs in the early universe. The cosmological FOPT proceeds with stochastic nucleations of true vacuum bubbles in the false vacuum environment followed by the rapid expansion until percolations via bubble collisions. The bubble wall collision and plasma fluid motion including sound waves and magnetohydrodynamic (MHD) turbulences would generate the corresponding SGWBs with broken power-law shapes in their energy density spectra.

Given the expansion history $a(t)$ and vacuum decay rate of form $\Gamma(t)\equiv A(t)e^{-B(t)}$ per unit time and unit volume, the fraction of spatial regions that are still staying at the false vacuum at time t can be estimated by [40, 41]

$$F(t;t_i)=\exp\left[-\frac{4\pi}{3}\int_{t_i}^{t}\mathrm{d}t'\,\Gamma(t')a(t')^3r(t,t')^3\right],\quad (4)$$

where t_i is the earliest possible time for the nucleation of the first bubble ever, and $r(t,t')=\int_{t'}^{t}\mathrm{d}\tilde{t}/a(\tilde{t})$ is the comoving radius of a bubble at time t nucleated from an earlier time t'. It is obvious that all regions are in the false vacuum before time t_i, namely $F(t<t_i;t_i)=1$. With the help of $F(t;t_i)$, the percolation time t_* for the GW spectra from the FOPT is then conventionally defined by $F(t_*;t_i)=0.7$ [42], around which the decay rate can be expanded linearly in time for its exponent as $\Gamma(t)=A(t_*)e^{-B(t_*)+\beta(t-t_*)}\equiv\Gamma_0e^{\beta t}$.

If most of bubbles collide with each other while bubble wall is still rapidly accelerating [43], then the GW spectrum is dominated by bubble wall collisions [44–48],

$$h^2\Omega_{\mathrm{env}}=1.67\times10^{-5}\left(\frac{100}{g_{\mathrm{dof}}}\right)^{\frac{1}{3}}\left(\frac{H_*}{\beta}\right)^2\left(\frac{\kappa_\phi\alpha}{1+\alpha}\right)^2\times\frac{0.11v_w^3}{0.42+v_w^2}\frac{3.8(f/f_{\mathrm{env}})^{2.8}}{1+2.8(f/f_{\mathrm{env}})^{3.8}},\quad (5)$$

with the peak frequency

$$\frac{f_{\mathrm{env}}}{\mathrm{Hz}}=1.65\times10^{-5}\left(\frac{g_{\mathrm{dof}}}{100}\right)^{\frac{1}{6}}\frac{T_*}{100\,\mathrm{GeV}}\frac{0.62(\beta/H_*)}{1.8-0.1v_w+v_w^2}.\quad (6)$$

If most of bubbles collide with each other at a constant terminal velocity, then the GW spectrum is dominated by sound waves [49–51] (the sub-dominated contribution from MHD turbulences is neglected),

$$h^2\Omega_{\mathrm{sw}}=2.65\times10^{-6}\left(\frac{100}{g_{\mathrm{dof}}}\right)^{\frac{1}{3}}\frac{H_*}{\beta}\left(\frac{\kappa_v\alpha}{1+\alpha}\right)^2\times\frac{7^{7/2}v_w(f/f_{\mathrm{sw}})^3}{(4+3(f/f_{\mathrm{sw}})^2)^{7/2}},\quad (7)$$

with the peak frequency

$$\frac{f_{\mathrm{sw}}}{\mathrm{Hz}}=1.9\times10^{-5}\left(\frac{g_{\mathrm{dof}}}{100}\right)^{\frac{1}{6}}\frac{T_*}{100\,\mathrm{GeV}}\frac{1}{v_w}\frac{\beta}{H_*}.\quad (8)$$

For our holographic approach, β/H_* is a free parameter, but all other parameters like $T_*=276.5$ MeV, $\alpha\equiv\Delta V/\rho_r=0.939$, $g_{\mathrm{dof}}\equiv\rho_r/\frac{\pi^2}{30}T_*^4=3.64$ are fixed by the holographic thermodynamics. The bubble wall velocity at collisions $v_w=0.9$ and efficency factors $\kappa_\phi=1$ (see [43] for an exact evaluation) and $\kappa_v=\alpha/(0.73+0.083\sqrt{\alpha}+\alpha)$ [52] are set for illustration since their precise values would not significantly change our conclusions [53]. While we are not able to compute β/H_* from first principle, it can be constrained by the PBH abundance associated with the FOPT. The SGWB spectra from our holographic model are shown in the left panel of Fig. 3, where the expected sensitivity curves of future GW observatories are included. One can find that the SGWBs are within the reach of IPTA and SKA when the associated PBH abundance saturates the current observational bound from LVC constraints.

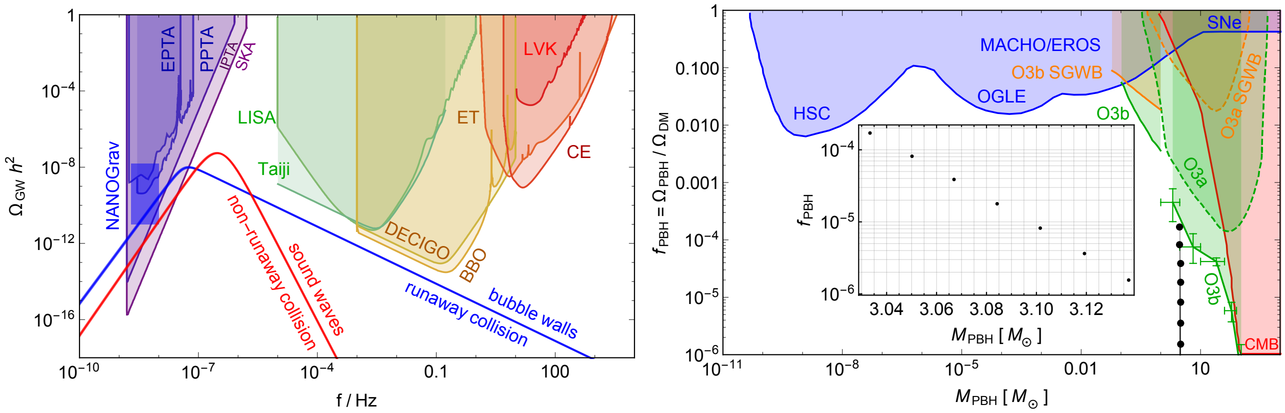

FIG. 3. The predictions for SGWB (left) and PBH (right) productions from our holographic pure gluon model. In the left panel, the GW contributions from sound waves (red curve) and wall collisions (blue curve) are obtained for the associated largest PBH abundance allowed by the current observational constraints shown in the right panel. In the right panel, the current PBH constraints [36] are updated by including the constraints from LVC O3a data [37] and O3b data [38, 39], and the insert zooms in the predicted PBH abundance regions.

PBH productions— We then turn to the PBH productions. To evaluate the probability for the postponed vacuum decay, note that the differential probability for a Hubble-sized region $V_H(t) = \frac{4}{3}\pi H(t)^{-3}$ not to decay at time t reads $\mathrm{d}P(t) = 1 - \Gamma(t)V_H(t)\mathrm{d}t \approx \exp\left[-\Gamma(t)V_H(t)\mathrm{d}t\right]$, then the probability for this Hubble volume not to decay until time t_n is obtained as

$$P(t_n) = \prod_{t=t_i}^{t_n} \mathrm{d}P(t) = \exp\left[-\int_{t_i}^{t_n} \mathrm{d}t\, V_H(t)\Gamma(t)\right]. \quad (9)$$

$P(t_n)$ is nothing but the PBH abundance $\Omega_{\rm PBH}$ at PBH formations if the overdensity in these Hubble volumes with postponed decay reach the PBH formation threshold δ_c,

$$\delta(t_{\rm PBH}) = \frac{\rho_r(t_{\rm PBH};t_n) + \rho_v(t_{\rm PBH};t_n)}{\rho_r(t_{\rm PBH};t_i) + \rho_v(t_{\rm PBH};t_i)} - 1 = \delta_c\,. \quad (10)$$

Here the vacuum energy densities inside and outside these Hubble volumes are estimated by $\rho_v(t;t_n) = F(t;t_n)\Delta V$ and $\rho_v(t;t_i) = F(t;t_i)\Delta V$, respectively, and the radiation energy densities inside and outside these Hubble volumes are solved from

$$\frac{\mathrm{d}}{\mathrm{d}t}\rho_r(t;t_n) + 4H(t;t_n)\rho_r(t;t_n) = -\frac{\mathrm{d}}{\mathrm{d}t}\rho_v(t;t_n)\,, \quad (11)$$

$$\frac{\mathrm{d}}{\mathrm{d}t}\rho_r(t;t_i) + 4H(t;t_i)\rho_r(t;t_i) = -\frac{\mathrm{d}}{\mathrm{d}t}\rho_v(t;t_i)\,, \quad (12)$$

respectively, where the Hubble parameters inside and outside these Hubble volumes are defined by $3M_{\rm Pl}^2 H(t;t_n)^2 = \rho_r(t;t_n) + \rho_v(t;t_n)$ and $3M_{\rm Pl}^2 H(t;t_i)^2 = \rho_r(t;t_i) + \rho_v(t;t_i)$, respectively. We adopt the analytic estimation [54] on the PBH threshold $\delta_c = \sin^2[\pi\sqrt{w}/(1+3w)] = 0.1786$ with the EoS $w = 0.0219$ evaluated from the dominant component at PBH formation. Finally, the PBH abundance at matter-radiation equality is estimated by $f_{\rm PBH} \equiv (a_{\rm eq}/a_{\rm PBH})\Omega_{\rm PBH}/\Omega_{\rm DM}(a_{\rm eq})$ and the PBH mass is estimated as $M_{\rm PBH} = 4\pi\gamma_{\rm PBH}M_{\rm Pl}^2/H_{\rm PBH}$ with usual PBH formation efficiency factor $\gamma_{\rm PBH} = 0.2$ [55]. The PBH mass function $f_{\rm PBH}(M_{\rm PBH})$ is shown in the right panel of Fig. 3 with respect to current PBH constraints. It is worth noting that for PBH formations, β is the only free parameter from our holographic approach, which could be constrained as $\beta/H_* > 8.59$ from the current GWTC-3 data by $f_{\rm PBH} < 0.00045$ in the mass range $[1\,M_\odot, 3\,M_\odot]$ [39]. Higher values for β/H_* are certainly allowable like those in Ref. [56] but with much more negligible PBH abundances and higher peak frequency and lower peak amplitude in the SGWBs that would be of less interest from both PBH and SGWB observations.

Conclusion and discussion— We have built up a holographic model for a pure gluon system to quantitatively confront the lattice data of SU(3) thermodynamics. It provides an effective model to capture the main feature of QCD matter, for which non-perturbative effects could be effectively adopted into the model parameters by matching with up-to-date lattice QCD. The resulting Polyakov loop operator and gluon condensation quantitatively match the lattice simulation, suggesting that there is a first-order confinement/deconfinement PT. The transition temperature is $T_c = 276.5$MeV as expected in lattice QCD literature. We have shown the GW energy spectrum and PBHs productions associated with the FOPT. With the most optimistic case constrained by the current PBH abundance, the energy spectrum of SGWBs could be potentially detectable within the sensitivity ranges of IPTA and SKA in the near future.

Since our holographic model can quantitatively capture the characteristic properties of the strong first-order confinement/deconfinement PT in a pure gluon system, one can study the transport properties in pure gluon and glueball gas to confirm the transition from a hydrodynamical point of view. It is worth considering real-time dynamics far from equilibrium, which is beyond the scope of lattice QCD. Moreover, it is an interesting direction to set up a holographic glueball action to compare the resulting glueball spectra with more experimental and lattice data. Furthermore, the present results, particularly those regarding the confinement/deconfinement PT, should be embedded into the framework of a general and hybrid QCD phase diagram, including, for example, an external magnetic field and a rotation.

Note added—While this work was being completed, the work [56] appeared in arXiv discussing the GWs from the confinement transition of a pure gluon sector. They consider a more complicated holographic setup that can fit the lattice data qualitatively and leave the phase transition temperature as a free parameter.

We thank Qing-Guo Huang, Yi-Fan Wang, Zu-Cheng Chen, Shi Pu, Yong Cai and Peng Liu for stimulating discussions. This work is supported in part by National Key Research and Development Program of China Grant No. 2021YFC2203004 and No. 2020YFC2201501, the National Natural Science Foundation of China Grants No. 12075101, No. 12122513, No. 12075298, No. 12047569, No. 11991052, No. 12047503, No. 12105344 and No. 11947233, the Key Research Program of the Chinese Academy of Sciences (CAS) Grant NO. XDPB15, the CAS Project for Young Scientists in Basic Research YSBR-006, the Science Research Grants from the China Manned Space Project with No. CMS-CSST-2021-B01. S.H. also would like to appreciate the financial support from Jilin University and Max Planck Partner group. We also acknowledge the use of the HPC Cluster of ITP-CAS.

Appendix A Thermodynamics and model parameters fixing

Substituting the ansatz (2), we obtain the following independent equations of motion (EoM).

$$\begin{aligned} \phi'' + \left(\frac{f'}{f} - \frac{\eta'}{2} + \frac{3}{r}\right)\phi' - \frac{1}{f}\partial_\phi V = 0, \\ \frac{\eta'}{r} + \frac{1}{3}\phi'^2 = 0, \\ \frac{2}{r}\frac{f'}{f} - \frac{\eta'}{r} + \frac{2}{3f}V + \frac{4}{r^2} = 0, \end{aligned} \tag{13}$$

where the prime denotes the derivative with respect to r. In what follows we will specify $V(\phi)$ as

$$V(\phi) = \left(6\gamma^2 - \frac{3}{2}\right)\phi^2 - 12\cosh(\gamma\phi), \tag{14}$$

where γ is the only free parameter. Note, however, that to fit the EoS for (2+1)-flavor QCD at zero baryon density, one has to introduce two free parameters [57] and three free parameters [58] in $V(\phi)$.

Near the AdS boundary $r \to \infty$ where $\phi \to 0$, one has

$$V(\phi) = -12 - \frac{3}{2}\phi^2 + \mathcal{O}(\phi^4)\,. \tag{15}$$

Therefore, the cosmological constant is given by $\Lambda = -6$ (the AdS radius $L = 1$) and the scaling dimension of the dual scalar operator is $\Delta = 3$. We then obtain the following asymptotic expansion:

$$\begin{aligned} \phi(r) &= \frac{\phi_s}{r} + \frac{\left(\gamma^4 - 1/6\right)\phi_s^3 \ln r + \phi_v}{r^2} + \ldots\,, \\ \eta(r) &= \frac{\phi_s^2}{6r^2} + \frac{(1-6\gamma^4)(1-12\ln r)\phi_s^4 + 72\phi_s\phi_v}{144r^4} + \ldots, \\ f(r) &= r^2 + \frac{\phi_s^2}{6} + \frac{2f_v - \phi_s^4(1-6\gamma^4)\ln r}{12r^2} + \ldots\,, \end{aligned} \tag{16}$$

where we have taken the normalization such that $\eta(r \to \infty) = 0$. ϕ_s is the source of the scalar operator of the boundary theory, which essentially breaks the conformal symmetry and plays the role of the energy scale.

To read off the physical observables, we incorporate the holographic renormalization by adding the boundary terms that are given as [59]

$$S_\partial = \frac{1}{2\kappa_N^2}\int \mathrm{d}x^4 \left[2K - 6 - \frac{\phi^2}{2} - \left(b + \frac{6\gamma^4 - 1}{12}\ln r\right)\phi^4\right] \tag{17}$$

at the AdS boundary $r \to \infty$. Here $h_{\mu\nu}$ is the induced metric and $K_{\mu\nu}$ is the extrinsic curvature defined by the outward pointing normal vector to the boundary.

The energy-momentum tensor of the dual boundary theory reads

$$\begin{aligned} T_{\mu\nu} &= \lim_{r\to\infty} \frac{2\,r^2}{\sqrt{-h}} \frac{\delta(S + S_\partial)_{on-shell}}{\delta h^{\mu\nu}} \\ &= \frac{1}{2\kappa_N^2} \lim_{r\to\infty} r^2 \Big[2(K h_{\mu\nu} - K_{\mu\nu} - 3h_{\mu\nu}) \\ &\quad - \left(\frac{1}{2}\phi^2 + \frac{6c_1^4 - 1}{12}\phi^4 \ln r + b\,\phi^4\right) h_{\mu\nu}\Big]\,. \end{aligned} \tag{18}$$

Inserting the UV expansion (16), we obtain

$$\begin{aligned}
\epsilon \equiv T_{tt} &= \frac{1}{2\kappa_N^2}\left(-3f_v + \phi_s\phi_v + \frac{1+48b}{48}\phi_s^4\right),\\
P \equiv T_{xx} &= \frac{1}{2\kappa_N^2}\left(-f_v + \phi_s\phi_v + \frac{3-48b-8\gamma^4}{48}\phi_s^4\right),\\
I \equiv \epsilon - 3P &= \frac{1}{2\kappa_N^2}\left(-2\phi_s\phi_v - \frac{1-24b-3\gamma^4}{6}\phi_s^4\right).
\end{aligned} \tag{19}$$

The temperature and entropy density are given by

$$T = \frac{1}{4\pi}f'(r_h)e^{-\eta(r_h)/2}, \quad s = \frac{2\pi}{\kappa_N^2}r_h^3, \tag{20}$$

where r_h is the location of the event horizon.

The free energy density F is identified as the temperature T times the renormalized action in the Euclidean signature.

$$\begin{aligned}
F &= \frac{T}{V}(S + S_\partial)^{\text{Euclidean}}_{\text{on-shell}},\\
&= \frac{1}{2\kappa_N^2}\left(f_v - \phi_s\phi_v - \frac{3-48b-8\gamma^4}{48}\phi_s^4\right).
\end{aligned} \tag{21}$$

with $V = \int \mathrm{d}x\mathrm{d}y\mathrm{d}z$. Taking advantage of radially conserved quantity

$$\mathcal{Q} = \frac{1}{2\kappa_N^2}r^5 e^{\eta/2}\left(\frac{f}{r^2}e^{-\eta}\right)', \tag{22}$$

and then evaluating at both horizon $r = r_h$ and UV boundary $r \to \infty$, we obtain the expected thermodynamic relation

$$F = \epsilon - T\,s = -P. \tag{23}$$

After obtaining the thermodynamic quantities, one can also compute some important transport coefficients, such as the speed of sound $c_s = \sqrt{\mathrm{d}P/\mathrm{d}\epsilon}$. These quantities are compared to the lattice results for pure gluon [28, 29, 32]. Then all free parameters of our holographic model can be fixed to be

$$\gamma = 0.735,\ \kappa_N^2 = 9.76\pi,\ \phi_s = 1.523\text{GeV},\ b = 0.06777.$$

The last parameter b that appears in the boundary term (17) corresponds to $P(T=0) = 0$. The fitting results are presented in Fig. 1 in the main text, from which there is a first-order phase transition (FOPT) at $T_c = 276.5\,\text{MeV}$.

To understand the nature of this FOPT, we compute the expectation value of Polyakov loop operator $\langle\mathcal{P}\rangle$, which is a good order parameter to the deconfinement PT for pure gluon system [35]. The computation of Polyakov loops in holography was given in [60]. Note that here we adopt the effective string tension $\alpha_p = 17.5$ and the renormalization constant $C_p = 0.11$ [61]. Surprisingly, as shown in Fig. 1, $\langle\mathcal{P}\rangle$ from our model quantitatively agrees with the lattice data [32] above T_c and drops to zero below T_c, suggesting that the FOPT from our model is a confinement/deconfinement PT.

Appendix B Computations of gluon condensation

To study the gluon condensation in our pure gluon model, we adopt a probe scalar field $\chi(r)$ on the background (2). The action reads

$$S = \frac{1}{2\kappa_N^2}\int \mathrm{d}^5x\sqrt{-g^s}e^{-\sqrt{\frac{3}{8}}\phi}\left[-\frac{1}{2}\nabla_\mu\chi\nabla^\mu\chi - \frac{1}{2}m_\chi^2\chi^2\right]. \tag{24}$$

Here g^s is the determinant of the metric in the string frame with

$$g^s_{\mu\nu} = e^{\sqrt{\frac{2}{3}}\phi}g_{\mu\nu}, \tag{25}$$

where $g_{\mu\nu}$ is the metric in the Einstein frame used in the previous section.

Then, the EoM of $\chi(r)$ is given by

$$\chi'' + \frac{1}{4}\left(\frac{12}{r} + \frac{4f'}{f} - 2\eta' + \sqrt{6}\phi'\right)\chi' - \frac{e^{\sqrt{\frac{2}{3}}\phi}}{f}m_\chi^2\chi = 0. \tag{26}$$

One considers the regular boundary condition on the IR:

$$\chi(r) = c_0 + c_1(r - r_h) + c_2(r - r_h)^2 + \dots, \tag{27}$$

The UV expansion shows

$$\chi(r) = \chi_0 r^{\Delta-4} + \dots + \chi_4 r^{-\Delta} + \dots. \tag{28}$$

The source χ_0 will be fixed to be a constant and then the holographic renormalized gluon condensation

$$\chi_4 = \langle G^2\rangle. \tag{29}$$

On the other hand, the subtracted gluon condensation $\delta\left\langle\frac{\beta(g)}{2g}G^2\right\rangle_T$ is related to the trace anomaly [62, 63]

$$\delta\left\langle\frac{\beta(g)}{2g}G^2\right\rangle_T \equiv \left\langle\frac{\beta(g)}{2g}G^2\right\rangle_T - \left\langle\frac{\beta(g)}{2g}G^2\right\rangle_0 = \epsilon - 3P, \tag{30}$$

where the coefficient $\beta(g)$ is the β-function of QCD and $\left\langle\frac{\beta(g)}{2g}G^2\right\rangle_0$ is determined by the exploration value of $\left\langle\frac{\beta(g)}{2g}G^2\right\rangle_T$ from finite temperature. For simplicity, we directly call $\delta\left\langle\frac{\beta(g)}{2g}G^2\right\rangle_T$ as physical gluon condensation in the main context. Following [24], we choose the renormalized dimension of the gluon operator $\Delta = 3.93$, which in turn determines the mass of bulk scalar via $m_\chi^2 = \Delta(\Delta - 4)$.

The β-function to 3-loop is given by [64]

$$\beta(g) = -\beta_0 g^3 - \beta_1 g^5 - \beta_2 g^7 + O(g^9)\,. \qquad (31)$$

Therefore, the coefficient in (30) reads

$$\frac{\beta(g)}{2g} = -\left(2\pi\beta_0\alpha_s + 8\pi^2\beta_1\alpha_s^2 + 32\pi^3\alpha_s^3\right)\,, \qquad (32)$$

with [65]

$$\alpha_s(T) = \frac{1}{4\pi\beta_0 Q}\left[1 - \frac{\beta_1}{\beta_0^2}\frac{\ln Q}{Q} + \frac{\beta_1^2}{\beta_0^4 Q^2}\left((\ln Q)^2 - \ln Q - 1 + \frac{\beta_0\beta_2}{\beta_1^2}\right)\right]\,, \qquad (33)$$

where $Q = \ln(T^2/\Lambda_{QCD}^2)$ and

$$\beta_0 = \frac{1}{(4\pi)^2}\left(11 - \frac{2}{3}N_f\right)\,,\ \beta_1 = \frac{1}{(4\pi)^4}\left(102 - \frac{38}{3}N_f\right)\,,$$
$$\beta_2 = \frac{1}{(4\pi)^6}\left(\frac{2857}{2} - \frac{5033}{18}N_f + \frac{325}{54}N_f^2\right)\,. \qquad (34)$$

The cutoff Λ_{QCD} gives the effective range of energy scale for $\alpha_s(T)$ which means $\alpha_s(T)$ only works for $T > \Lambda_{QCD}$. The temperature dependent gluon condensation is shown in Fig. 2 with $\Lambda_{QCD} = 0.14$GeV and $\chi_0 = -2.97 \times 10^{-10}\text{GeV}^{4-\Delta}$. The data for the trace anomaly from lattice QCD [28, 29] is included. It is clearly that our results match the lattice data pretty well.

Appendix C Computations of GWs and PBHs

We fill in some details for the PBH and SGWB productions associated with a FOPT and in particular for our holographic gluon model. The process of bubble nucleations and collisions mixed with PBH productions is highly inhomogeneous, therefore, a rigorous treatment would require for numerical simulations. A convenient approximation to the background evolution is close to the radiation-dominated era with $a(t) \propto t^{1/2}$, which will be checked and confirmed later as a good approximation for the parameter space we consider. We also normalize all dimensional quantities with the dimensional input $\Gamma_0^{1/4}$, such as $\bar{t} \equiv \Gamma_0^{1/4} t$, $\bar{\beta} \equiv \beta/\Gamma_0^{1/4}$, and $\bar{\alpha} \equiv \Delta V/(3M_{\rm Pl}^2\Gamma_0^{1/2})$.

During the asynochronized progress of PT, the fraction of spatial regions that are still staying at the false vacuum at time t is now computed as

$$F(\bar{t};\bar{t}_i,\bar{\beta}) = \exp\left[-\frac{4}{3}\pi\int_{\bar{t}_i}^{\bar{t}} \mathrm{d}\bar{t}' 8 e^{\bar{\beta}\bar{t}'}\left(\sqrt{\bar{t}\bar{t}'} - \bar{t}'\right)^3\right]. \qquad (35)$$

Without loss of generality, we can choose the true vacuum as the zero point of the potential energy so that the vacuum energy in the normal decay regions and delayed decayed regions are estimated by $\rho_v(\bar{t};\bar{t}_i) = F(\bar{t};\bar{t}_i)\Delta V$ and $\rho_v(\bar{t};\bar{t}_n) = F(\bar{t};\bar{t}_n)\Delta V$, respectively. The time evolution for the spatial fraction of false vacuum regions in the normal (solid curves) and delayed (dotted curves) decay channels is shown in the top panel of Fig. 4. For a larger value of $\bar{\beta}$, the PT proceeds more abruptly. For a smaller value of $\bar{\beta}$, the PT proceeds more slowly.

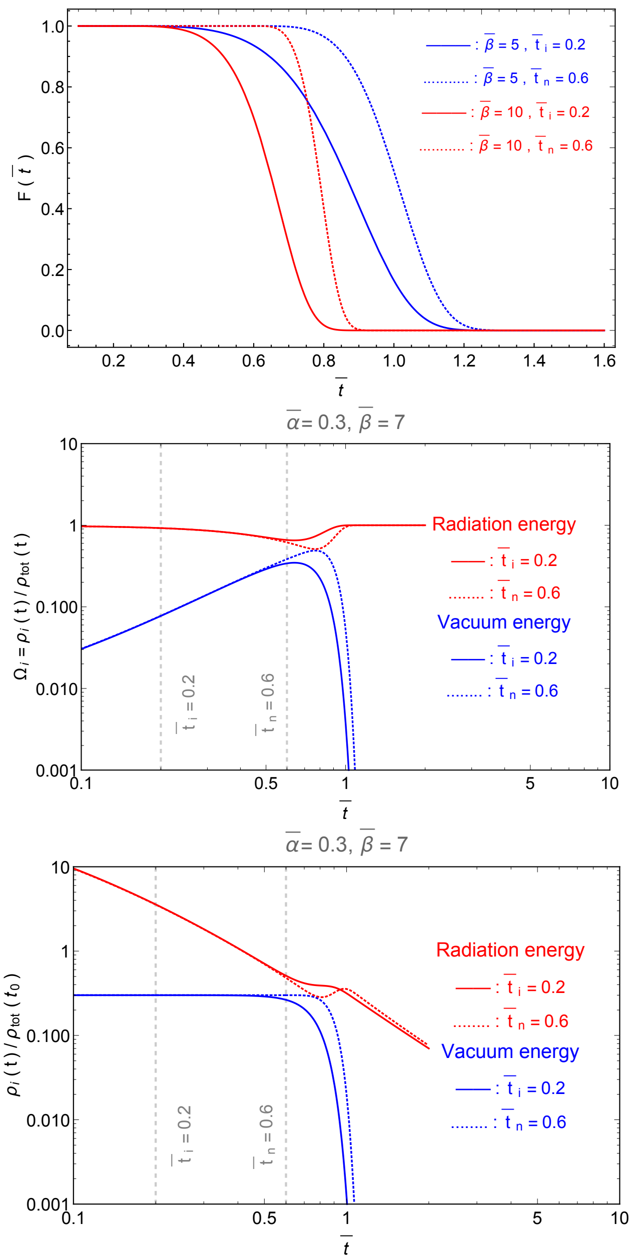

FIG. 4. The time evolution for the spatial fraction of false vacuum regions (top), the radiation and vacuum energy density fractions (medium) and the radiation and vacuum energy densities normalized by the total energy density at some time $\bar{t}_0 = 1/2$ (bottom). In all panels, $\bar{t}_i = 0.2$ and $\bar{t}_n = 0.6$ denote the normal decay channel and delayed decay channel, respectively.

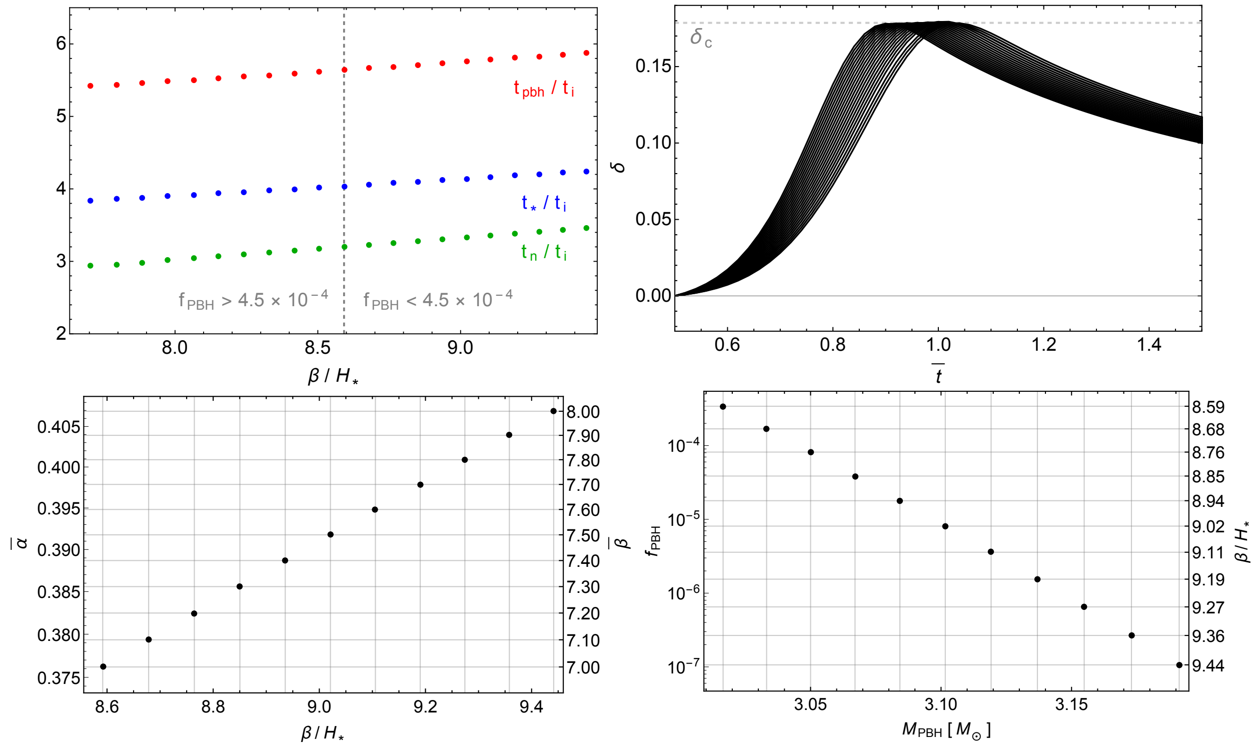

FIG. 5. The results for the parameters in producing the SGWB and PBHs. *Upper left*: The delayed decay time t_n (green), the percolation time t_* (blue), and the PBH formation time $t_{\rm PBH}$ (red) after normalized to the normal decay time t_i with respect to the parameter regime of β/H_* of interest. *Upper right*: The time evolution of overdensity with respect to the parameter regime of β/H_* of interest. *Lower left*: The parameter space for $\bar{\alpha}$ and β/H_* with respect to the input parameter $\bar{\beta}$. *Lower right*: The parameter space for $f_{\rm PBH}$ and $M_{\rm PBH}$ with respect to the parameter regime of β/H_* of interest.

However, the rest of energy density does not evolve exactly as radiations due to the interrupt of the PT process and associated PBH productions. Nevertheless, the radiation evolution could be effectively solved from

$$\frac{\mathrm{d}\bar{\rho}_r}{\mathrm{d}\bar{t}}+4\bar{\rho}_r\sqrt{\bar{\rho}_r+\bar{\rho}_v}=-\bar{\alpha}\frac{\mathrm{d}F}{\mathrm{d}\bar{t}}, \tag{36}$$

with abbreviations $\bar{\rho}_r \equiv \rho_r/(3M_{\rm Pl}^2\Gamma_0^{1/2})$ and $\bar{\rho}_v \equiv \rho_v/(3M_{\rm Pl}^2\Gamma_0^{1/2}) = F\bar{\alpha}$. Note that Γ_0 naturally defines a time t_0 in such a way that $H(t_0)=\Gamma_0^{1/4}$. Our assumption for radiation dominance requires $\bar{t}_0 = H(t_0)t_0 = 1/2$. Then the initial condition is chose as $\bar{\rho}_r(\bar{t}_0)=1-\bar{\rho}_v(\bar{t}_0)$. For given $\bar{\alpha}$ and $\bar{\beta}$, Eq. 36 can be solved for the normal and delayed decay channels respectively with $\bar{t}_n > \bar{t}_i$. It can be checked numerically that, as long as $\bar{\alpha} < 0.5$, our assumption for the radiation dominance is valid throughout the whole process of PT as shown in the medium and bottom panels of Fig. 4 for the radiation/vacuum energy density fractions and radiation/vacuum energy densities normalized by the total energy density at the time $\bar{t}_0 = 1/2$, respectively. The normal decay time $\bar{t}_i = 0.2$ and delayed decay time $\bar{t}_n = 0.6$ as well as $\bar{\alpha} = 0.3$ and $\bar{\beta} = 7$ are chose for illustration.

With the full solutions for the radiation and vacuum energy densities in the normal and delayed decay regions, the overdensity of total energy density in the delayed decay regions can be directly evaluated by

$$\delta(\bar{t})=\frac{\bar{\rho}_r(\bar{t};\bar{t}_n)+\bar{F}(\bar{t};\bar{t}_n)\bar{\alpha}}{\bar{\rho}_r(\bar{t};\bar{t}_i)+\bar{F}(\bar{t};\bar{t}_i)\bar{\alpha}}-1\,. \tag{37}$$

The time evolution of $\delta(\bar{t};\bar{t}_i,\bar{t}_n,\bar{\alpha},\bar{\beta})$ is first increasing due to the gradual accumulation of energy density in false vacuum and then decreasing due to the rapid declination of volume fraction in false vacuum. For given $\bar{t}_i$, $\bar{\alpha}$ and $\bar{\beta}$, when the maximal overdensity exactly saturates a given PBH threshold δ_c, we can solve for the required delayed decay time $\bar{t}_n$, from which the PBH formation time is then solved from $\delta(\bar{t}_{\rm PBH};\bar{t}_i,\bar{t}_n,\bar{\alpha},\bar{\beta})=\delta_c$. Although suffered from large uncertainties of numerical simulations, we can adopt the analytic estimation [54] on the PBH threshold via $\delta_c=\sin^2[\pi\sqrt{w}/(1+3w)]$ with the EoS w evaluated from the dominant component at PBH formation.

The PBH mass produced from our postponed decay mechanism is almost monochromatic since the numerical simulations for the gravitational collapse of over-dense regions with sub-horizon size are still missing. We therefore only focus on the PBH mass collapsed from the over-dense Hubble volumes with postponed decay,

$$\frac{M_{\rm PBH}}{M_\odot} = 4\pi\gamma_{\rm PBH}\left(\frac{M_{\rm Pl}}{M_\odot}\right)\left(\frac{M_{\rm Pl}/\Gamma_0^{1/4}}{H_{\rm PBH}/\Gamma_0^{1/4}}\right), \tag{38}$$

where $\gamma_{\rm PBH} = 0.2$ [55], $M_{\rm Pl}/M_\odot = 2.182\times 10^{-39}$, and $\bar{H}_{\rm PBH} \equiv H_{\rm PBH}/\Gamma_0^{1/4} = \sqrt{\bar\rho_{\rm tot}(\bar t_{\rm PBH};\bar t_n)}$. The other factor $M_{\rm Pl}/\Gamma_0^{1/4}$ can be roughly estimated as

$$\frac{\Gamma_0^{1/4}}{M_{\rm Pl}} = \left(\frac{\pi^2}{90}g_{\rm dof}\right)^{1/2}\left(\frac{T_*}{M_{\rm Pl}}\right)^2 e^{-\frac{\beta}{8H_*}} \tag{39}$$

by noting that the percolation time defined by $F(t_*;t_i) = 0.7$ is usually close to the time when the bubble nucleation rate balances the Hubble expansion rate $\Gamma(t_*)\approx H(t_*)^4$, thus, $\Gamma_0 \approx H_*^4 e^{-\beta t_*}$ followed by the replacements of $3M_{\rm Pl}^2H_*^2 = (\pi^2/30)g_{\rm dof}T_*^4$ and $H_*t_* = 1/2$ due to the radiation dominance.

The PBH abundance $f_{\rm PBH} = (a_{\rm eq}/a_{\rm PBH})\Omega_{\rm PBH}/\Omega_{\rm DM}^{\rm eq}$ normalized to the dark matter fraction $\Omega_{\rm DM}^{\rm eq} = 0.42$ at the matter-radiation equality is then estimated by

$$\Omega_{\rm PBH} = \exp\left[-\frac{4}{3}\pi\int_{\bar t_i}^{\bar t_n}{\rm d}\bar t\, e^{\bar\beta\bar t}\left(\frac{\sqrt{\bar t/\bar t_{\rm PBH}}}{\bar H_{\rm PBH}}\right)^3\right], \tag{40}$$

where the redshift factor $a_{\rm eq}/a_{\rm PBH} = T_{\rm PBH}/T_{\rm eq}$ with $T_{\rm eq}\approx 0.75$ eV can be estimated by inserting $3M_{\rm Pl}^2H_{\rm PBH}^2 = (\pi^2/30)g_{\rm dof}T_{\rm PBH}^4$ after replacing $H_{\rm PBH} = \bar H_{\rm PBH}\Gamma_0^{1/4}$ with previously computed $\bar H_{\rm PBH}$ and $\Gamma_0^{1/4}$, namely,

$$T_{\rm PBH} = T_*\sqrt{\bar H_{\rm PBH}}e^{-\frac{\beta}{16H_*}}. \tag{41}$$

Note that the $g_{\rm dof}$-dependence in $T_{\rm PBH}$ and Γ_0 cancels out, leaving no dependence on $g_{\rm dof}$ for the PBH abundance. Finally, in computing both PBH mass and abundance, the inverse duration is determined by $\beta/H_* = \bar\beta/\sqrt{\bar\rho_{\rm tot}(\bar t_*;\bar t_i)}$.

For our holographic model of gluondynamics, β is the only free parameter since one can further fix $\bar\alpha$ from matching the strength factor $\alpha = \bar\alpha/\bar\rho_r(\bar t_*;\bar t_i)$ to the value 0.939 obtained from holographic calculations. The other inputs from holographic calculations include the PT temperature $T_* = 276.5$ MeV, the effective degrees of freedom $g_{\rm dof} = 3.64$ and the PBH threshold $\delta_c = 0.1786$ from the EoS $w = 0.0219$ of the dominant component in the unbroken phase[54]. The final results are summarized in Fig. 5. In the first panel, all the characteristic time scales, such as the delayed decay time t_n, the percolation time t_*, and the PBH formation time $t_{\rm PBH}$, are shown with respect to β/H_* after normalized to the normal decay time t_i. In the second panel, the time evolution of the overdensity within the delayed decay regions are shown to exactly saturate the PBH formation threshold. In the third and last panels, the parameter space for $\bar\alpha$, β/H_*, $f_{\rm PBH}$, and $M_{\rm PBH}$ are shown with respect to the input free parameter $\bar\beta$. It is worth noting that the current constraint from the current GWTC-3 data [39] on the PBH abundance $f_{\rm PBH} < 0.00045$ in the mass range $[1\,M_\odot, 3\,M_\odot]$ would constrain $\beta/H_* > 8.59$.

* hesong@jlu.edu.cn
† liliphy@itp.ac.cn
‡ lizhibin@zzu.edu.cn
§ schwang@itp.ac.cn

[1] R.-G. Cai, Z. Cao, Z.-K. Guo, S.-J. Wang, and T. Yang, "The Gravitational-Wave Physics," Natl. Sci. Rev. **4** no. 5, (2017) 687–706, arXiv:1703.00187 [gr-qc].
[2] C. Caprini et al., "Detecting gravitational waves from cosmological phase transitions with LISA: an update," JCAP **03** (2020) 024, arXiv:1910.13125 [astro-ph.CO].
[3] M. B. Hindmarsh, M. Lüben, J. Lumma, and M. Pauly, "Phase transitions in the early universe," SciPost Phys. Lect. Notes **24** (2021) 1, arXiv:2008.09136 [astro-ph.CO].
[4] L. Bian et al., "The Gravitational-wave physics II: Progress," Sci. China Phys. Mech. Astron. **64** no. 12, (2021) 120401, arXiv:2106.10235 [gr-qc].
[5] R.-G. Cai, K. Hashino, S.-J. Wang, and J.-H. Yu, "Gravitational waves from patterns of electroweak symmetry breaking: an effective perspective," arXiv:2202.08295 [hep-ph].
[6] J. Liu, L. Bian, R.-G. Cai, Z.-K. Guo, and S.-J. Wang, "Primordial black hole production during first-order phase transitions," Phys. Rev. D **105** no. 2, (2022) L021303, arXiv:2106.05637 [astro-ph.CO].
[7] J. Liu, L. Bian, R.-G. Cai, Z.-K. Guo, and S.-J. Wang, "Constraining first-order phase transitions with curvature perturbations," arXiv:2208.14086 [astro-ph.CO].
[8] K. Hashino, S. Kanemura, and T. Takahashi, "Primordial black holes as a probe of strongly first-order electroweak phase transition," arXiv:2111.13099 [hep-ph].
[9] M. J. Baker, M. Breitbach, J. Kopp, and L. Mittnacht, "Primordial Black Holes from First-Order Cosmological Phase Transitions," arXiv:2105.07481 [astro-ph.CO].
[10] M. J. Baker, M. Breitbach, J. Kopp, and L. Mittnacht, "Detailed Calculation of Primordial Black Hole Formation During First-Order Cosmological Phase Transitions," arXiv:2110.00005 [astro-ph.CO].
[11] K. Kawana and K.-P. Xie, "Primordial black holes from a cosmic phase transition: The collapse of Fermi-balls," Phys. Lett. B **824** (2022) 136791, arXiv:2106.00111 [astro-ph.CO].
[12] P. Huang and K.-P. Xie, "Primordial black holes from an electroweak phase transition," arXiv:2201.07243 [hep-ph].
[13] D. Marfatia and P.-Y. Tseng, "Correlated signals of first-order phase transitions and primordial black hole evaporation," arXiv:2112.14588 [hep-ph].
[14] E. V. Shuryak, "Two stage equilibration in high-energy heavy ion collisions," Phys. Rev. Lett. **68** (1992) 3270–3272.

[15] L. D. McLerran and R. Venugopalan, "Computing quark and gluon distribution functions for very large nuclei," Phys. Rev. D **49** (1994) 2233–2241, arXiv:hep-ph/9309289.

[16] J. Alam, B. Sinha, and S. Raha, "Successive equilibration in quark - gluon plasma," Phys. Rev. Lett. **73** (1994) 1895–1898.

[17] **LHCb** Collaboration, R. Aaij et al., "Observation of $J/\psi p$ Resonances Consistent with Pentaquark States in $\Lambda_b^0 \to J/\psi K^- p$ Decays," Phys. Rev. Lett. **115** (2015) 072001, arXiv:1507.03414 [hep-ex].

[18] U. W. Heinz, "The Quark gluon plasma at RHIC," Nucl. Phys. A **721** (2003) 30–39, arXiv:nucl-th/0212004.

[19] Z. Xu and C. Greiner, "Thermalization of gluons in ultrarelativistic heavy ion collisions by including three-body interactions in a parton cascade," Phys. Rev. C **71** (2005) 064901, arXiv:hep-ph/0406278.

[20] W. Broniowski, W. Florkowski, M. Chojnacki, and A. Kisiel, "Free-streaming approximation in early dynamics of relativistic heavy-ion collisions," Phys. Rev. C **80** (2009) 034902, arXiv:0812.3393 [nucl-th].

[21] J. M. Maldacena, "The Large N limit of superconformal field theories and supergravity," Adv. Theor. Math. Phys. **2** (1998) 231–252, arXiv:hep-th/9711200.

[22] S. S. Gubser, I. R. Klebanov, and A. M. Polyakov, "Gauge theory correlators from noncritical string theory," Phys. Lett. B **428** (1998) 105–114, arXiv:hep-th/9802109.

[23] E. Witten, "Anti-de Sitter space and holography," Adv. Theor. Math. Phys. **2** (1998) 253–291, arXiv:hep-th/9802150.

[24] S. S. Gubser, A. Nellore, S. S. Pufu, and F. D. Rocha, "Thermodynamics and bulk viscosity of approximate black hole duals to finite temperature quantum chromodynamics," Phys. Rev. Lett. **101** (2008) 131601, arXiv:0804.1950 [hep-th].

[25] U. Gursoy, E. Kiritsis, L. Mazzanti, and F. Nitti, "Deconfinement and Gluon Plasma Dynamics in Improved Holographic QCD," Phys. Rev. Lett. **101** (2008) 181601, arXiv:0804.0899 [hep-th].

[26] M. Panero, "Thermodynamics of the QCD plasma and the large-N limit," Phys. Rev. Lett. **103** (2009) 232001, arXiv:0907.3719 [hep-lat].

[27] M. Järvinen, "Holographic modeling of nuclear matter and neutron stars," arXiv:2110.08281 [hep-ph].

[28] G. Boyd, J. Engels, F. Karsch, E. Laermann, C. Legeland, M. Lutgemeier, and B. Petersson, "Thermodynamics of SU(3) lattice gauge theory," Nucl. Phys. B **469** (1996) 419–444, arXiv:hep-lat/9602007.

[29] M. Caselle, A. Nada, and M. Panero, "QCD thermodynamics from lattice calculations with nonequilibrium methods: The SU(3) equation of state," Phys. Rev. D **98** no. 5, (2018) 054513, arXiv:1801.03110 [hep-lat].

[30] J. Kuti, J. Polonyi, and K. Szlachanyi, "Monte Carlo Study of SU(2) Gauge Theory at Finite Temperature," Phys. Lett. B **98** (1981) 199.

[31] L. D. McLerran and B. Svetitsky, "Quark Liberation at High Temperature: A Monte Carlo Study of SU(2) Gauge Theory," Phys. Rev. D **24** (1981) 450.

[32] S. Gupta, K. Huebner, and O. Kaczmarek, "Renormalized Polyakov loops in many representations," Phys. Rev. D **77** (2008) 034503, arXiv:0711.2251 [hep-lat].

[33] S. Borsanyi, G. Endrodi, Z. Fodor, S. D. Katz, and K. K. Szabo, "Precision SU(3) lattice thermodynamics for a large temperature range," JHEP **07** (2012) 056, arXiv:1204.6184 [hep-lat].

[34] To fix the energy scale, we also set the source of the scalar to be $\phi_s = 1.523$ GeV and the Newton constant to be $\kappa_N^2 = 9.76\pi$.

[35] K. Fukushima and V. Skokov, "Polyakov loop modeling for hot QCD," Prog. Part. Nucl. Phys. **96** (2017) 154–199, arXiv:1705.00718 [hep-ph].

[36] B. Carr and F. Kuhnel, "Primordial Black Holes as Dark Matter: Recent Developments," Ann. Rev. Nucl. Part. Sci. **70** (2020) 355–394, arXiv:2006.02838 [astro-ph.CO].

[37] G. Hütsi, M. Raidal, V. Vaskonen, and H. Veermäe, "Two populations of LIGO-Virgo black holes," JCAP **03** (2021) 068, arXiv:2012.02786 [astro-ph.CO].

[38] A. H. Nitz and Y.-F. Wang, "Broad search for gravitational waves from subsolar-mass binaries through LIGO and Virgo's third observing run," arXiv:2202.11024 [astro-ph.HE].

[39] Z.-C. Chen, C. Yuan, and Q.-G. Huang, "Confronting the primordial black hole scenario with the gravitational-wave events detected by LIGO-Virgo," arXiv:2108.11740 [astro-ph.CO].

[40] A. H. Guth and E. J. Weinberg, "Could the Universe Have Recovered from a Slow First Order Phase Transition?," Nucl. Phys. B **212** (1983) 321–364.

[41] M. S. Turner, E. J. Weinberg, and L. M. Widrow, "Bubble nucleation in first order inflation and other cosmological phase transitions," Phys. Rev. D **46** (1992) 2384–2403.

[42] V. K. Shante and S. Kirkpatrick, "An introduction to percolation theory," Advances in Physics **20** no. 85, (1971) 325–357. http://dx.doi.org/10.1080/00018737100101261.

[43] R.-G. Cai and S.-J. Wang, "Effective picture of bubble expansion," JCAP **03** (2021) 096, arXiv:2011.11451 [astro-ph.CO].

[44] A. Kosowsky, M. S. Turner, and R. Watkins, "Gravitational radiation from colliding vacuum bubbles," Phys. Rev. D **45** (1992) 4514–4535.

[45] A. Kosowsky, M. S. Turner, and R. Watkins, "Gravitational waves from first order cosmological phase transitions," Phys. Rev. Lett. **69** (1992) 2026–2029.

[46] A. Kosowsky and M. S. Turner, "Gravitational radiation from colliding vacuum bubbles: envelope approximation to many bubble collisions," Phys. Rev. D **47** (1993) 4372–4391, arXiv:astro-ph/9211004.

[47] M. Kamionkowski, A. Kosowsky, and M. S. Turner, "Gravitational radiation from first order phase transitions," Phys. Rev. D **49** (1994) 2837–2851, arXiv:astro-ph/9310044.

[48] S. J. Huber and T. Konstandin, "Gravitational Wave Production by Collisions: More Bubbles," JCAP **09** (2008) 022, arXiv:0806.1828 [hep-ph].

[49] M. Hindmarsh, S. J. Huber, K. Rummukainen, and D. J. Weir, "Gravitational waves from the sound of a first order phase transition," Phys. Rev. Lett. **112** (2014) 041301, arXiv:1304.2433 [hep-ph].

[50] M. Hindmarsh, S. J. Huber, K. Rummukainen, and D. J. Weir, "Numerical simulations of acoustically generated gravitational waves at a first order phase

transition," Phys. Rev. D **92** no. 12, (2015) 123009, arXiv:1504.03291 [astro-ph.CO].

[51] M. Hindmarsh, S. J. Huber, K. Rummukainen, and D. J. Weir, "Shape of the acoustic gravitational wave power spectrum from a first order phase transition," Phys. Rev. D **96** no. 10, (2017) 103520, arXiv:1704.05871 [astro-ph.CO]. [Erratum: Phys.Rev.D 101, 089902 (2020)].

[52] J. R. Espinosa, T. Konstandin, J. M. No, and G. Servant, "Energy Budget of Cosmological First-order Phase Transitions," JCAP **06** (2010) 028, arXiv:1004.4187 [hep-ph].

[53] S.-J. Wang and Z.-Y. Yuwen, "The energy budget of cosmological first-order phase transitions beyond the bag equation of state," JCAP **10** (2022) 047, arXiv:2206.01148 [hep-ph].

[54] T. Harada, C.-M. Yoo, and K. Kohri, "Threshold of primordial black hole formation," Phys. Rev. D **88** no. 8, (2013) 084051, arXiv:1309.4201 [astro-ph.CO]. [Erratum: Phys.Rev.D 89, 029903 (2014)].

[55] B. J. Carr, "The Primordial black hole mass spectrum," Astrophys. J. **201** (1975) 1–19.

[56] E. Morgante, N. Ramberg, and P. Schwaller, "Echo of the Dark: Gravitational Waves from Dark SU(3) Yang-Mills Theory," arXiv:2210.11821 [hep-ph].

[57] R.-G. Cai, S. He, L. Li, and Y.-X. Wang, "Probing QCD critical point and induced gravitational wave by black hole physics," arXiv:2201.02004 [hep-th].

[58] J. Grefa, J. Noronha, J. Noronha-Hostler, I. Portillo, C. Ratti, and R. Rougemont, "Hot and dense quark-gluon plasma thermodynamics from holographic black holes," Phys. Rev. D **104** no. 3, (2021) 034002, arXiv:2102.12042 [nucl-th].

[59] L. Li, "On Thermodynamics of AdS Black Holes with Scalar Hair," Phys. Lett. B **815** (2021) 136123, arXiv:2008.05597 [gr-qc].

[60] D. Bak, A. Karch, and L. G. Yaffe, "Debye screening in strongly coupled N=4 supersymmetric Yang-Mills plasma," JHEP **08** (2007) 049, arXiv:0705.0994 [hep-th].

[61] D. Li, S. He, M. Huang, and Q.-S. Yan, "Thermodynamics of deformed AdS_5 model with a positive/negative quadratic correction in graviton-dilaton system," JHEP **09** (2011) 041, arXiv:1103.5389 [hep-th].

[62] P. Gubler and D. Satow, "Recent Progress in QCD Condensate Evaluations and Sum Rules," Prog. Part. Nucl. Phys. **106** (2019) 1–67, arXiv:1812.00385 [hep-ph].

[63] T. D. Cohen, R. J. Furnstahl, and D. K. Griegel, "Quark and gluon condensates in nuclear matter," Phys. Rev. C **45** (1992) 1881–1893.

[64] D. d'Enterria et al., "α_s(2019): Precision measurements of the QCD coupling," arXiv:1907.01435 [hep-ph].

[65] A. I. Alekseev, "Strong coupling constant to four loops in the analytic approach to QCD," Few Body Syst. **32** (2003) 193–217, arXiv:hep-ph/0211339.